Modeling Spray Atomization with the Kelvin-Helmholtz / Rayleigh-Taylor Hybrid Model

Jennifer C. Beale and Rolf D. Reitz

Engine Research Center
University of Wisconsin-Madison
Madison, WI 53706

Revised

Submitted to:
Atomization and Sprays
February 1999

Corresponding Author:
Prof. Rolf D. Reitz
Department of Mechanical Engineering
University of Wisconsin – Madison
Engine Research Center
1500 Engineering Drive
Madison Wisconsin 53703

Phone: (608) 262-0145
Fax: (608) 262-6707
E-mail: **reitz@engr.wisc.edu**

Abstract

An improved spray atomization model is presented for use in both diesel and gasoline spray computations. The KH-RT hybrid atomization model consists of two distinct steps: primary and secondary break-up. The Kelvin-Helmholtz (KH) instability model was used to predict the primary break-up of the intact liquid core of a diesel jet. The secondary break-up of the individual drops was modeled with the Kelvin-Helmholtz model in conjunction with the Rayleigh-Taylor (RT) accelerative instability model. A modification was made to the KH-RT hybrid model that allowed the RT accelerative instabilities to affect all drops outside the intact liquid core of the jet. In previous implementations, only the drops beyond the break-up length are affected by RT break-up. Furthermore, a Rosin-Rammler distribution was used to specify the sizes of children drops after the RT break-up of a parent drop. The modifications made to the KH-RT hybrid model were found to give satisfactory results and to improve the temperature dependence of the liquid fuel penetration of the diesel sprays significantly. The KH-RT model was also found to predict the spray shape, penetration, and local SMD of hollow-cone sprays as well as previous gasoline spray models based on the TAB model.

Introduction

Automotive technology is growing rapidly and automobile manufacturers must constantly find new ways to keep up with their competitors. One of the more recent methods of staying abreast with new technological developments is through the use of computer modeling. In the past experiments were more convenient to optimize an engine, but today it would save time and money if a computer model could be used instead.

Although computational models can be used for many applications, they still need improvements. One of the goals of this study is to improve the spray modeling capabilities of CFD codes. There are many computational models of physical sub-processes in engine sprays. To simulate an engine, a code must be able to simulate not only the moving piston and airflow inside the combustion chamber, but also the fuel injection process, the ignition and chemical kinetics involved in combustion. There are other processes such as turbulence that are also influential. However, the main subject of this paper is the fuel injection process.

This paper considers sprays for both direct injection diesels and direct injection gasoline engines, which are being investigated as possible alternatives to the more common port injected gasoline engine in today's automobile market. A consideration was that it would be convenient if both kinds of fuel injection systems could be modeled with the same CFD code. Currently, different atomization models are used in multidimensional modeling to model low and high-pressure sprays [1, 2]. Since the physics of spray break-up are likely to be similar for the two applications, using one atomization model would help to reduce complexity and increase confidence in multi-dimensional spray models.

Since Rayleigh's pioneering work in the late nineteenth century, great progress has been made toward the understanding of jet behavior. The atomization process has been modeled in a

variety of ways. Monitoring the Kelvin-Helmholtz (KH) instability at the liquid-gas interface is commonly used to predict the break-up of a high-pressure liquid jet [2]. The Taylor Analogy Breakup (TAB) model, in which drop behavior is compared to an oscillating spring-mass system, is also commonly used. Hybrid models have been investigated as well (e.g. Pelloni and Bianchi [1]). The KH wave model has been combined with the TAB model or the newer Rayleigh-Taylor (RT) instability model (e.g. Patterson and Reitz [2]). Modifications to these models are often the subject of many studies and published papers.

Reitz and Bracco [3] evaluated a number of proposed jet atomization theories. Comparing these theories to experimental data, they found that none were adequate when used alone. They concluded that atomization was due to the aerodynamic effect of the gas on the injected liquid as well as due to nozzle geometry effects. The aerodynamic interaction of gas and liquid was described using the Kelvin-Helmholtz instability analysis. Reitz and Bracco [3] briefly mention the existence of a length of intact liquid near the nozzle of a jet. If the jet atomization theory they describe is correct, then an intact liquid core must exist inside the jet where it has not yet been affected by the surrounding air. Hiroyasu [4] performed an extensive study on the liquid break-up length. He showed through experimental analysis that the break-up length depends strongly on nozzle geometry effects and the injection velocity.

Models for the intact core are discussed by Bracco [5]. Reitz and Diwakar [6] simulated the intact core by injecting drops with an initial SMR equal to the effective nozzle radius. An actual continuous liquid region cannot be modeled in discrete particle spray models, therefore these large closely packed "blobs" were used to represent the intact portion of the spray. Reitz [7] used the "blob" injection model and incorporated a wave model based on the KH instability to predict secondary drop break-up. The new model was shown to predict "the presence of finely

atomized drops which are seen at the spray edge" in experimental photographs, as well as "an inner core of largely unbroken liquid." The latter has also been observed experimentally.

Currently, hybrid models are commonly used to represent drop break-up and atomization. Su et al. [8] combined the KH wave model with a model that considered Rayleigh-Taylor accelerative instabilities for the spray droplets. Su et al. found that the KH-RT model predicted a better drop size distribution and thus also calculated drop size trends closer to experimental data than the lone KH model. The experiments simulated included multiple injection spray cases where a decrease in drop size was observed between the two injected sprays. Although the KH model alone was not able to predict this decrease, the KH-RT model did predict the experimentally observed trend.

Ricart et al. [9] used the KH-RT model together with a break-up length concept. In his study, Hiroyaso [5] noted that break-up after a certain length occurs at a different rate than before this "core" length. Therefore, a break-up length was incorporated such that the RT model did not begin to compete with the KH model until after the drops had passed beyond this specified length, consistent with the view that droplet secondary break-up should only occur downstream of the intact liquid core near the nozzle. In the area within the break-up length only the KH-model was applied. Ricart et al. [9] determined the break-up length using an expression from Levich theory [10].

The development of hollow-cone spray break-up models has proceeded similarly to the development of high-pressure liquid jet atomization models. Before break-up models were introduced to CFD codes, it was common to assume an initial SMR at the nozzle exit that would yield the correct spray penetration. If the SMR downstream of the nozzle is known from experimental measurements, this method works well for engine simulations. However, although

this method is simple, it is not always accurate, since it neglects spray processes between the nozzle exit and the measurement station such as evaporation and drop coalescence.

Using the TAB model, O'Rourke and Amsden [11] performed a study on the effect of drop break-up on both hollow-cone and solid-cone sprays. They concluded that drop break-up does significantly affect sprays and that it is necessary to be included for spray modeling. Currently, the TAB model is standard in most versions of the KIVA code [12]. However, improvements on this model are constantly in progress and are the subject of many papers.

Han et al. [13] proposed modifications to the TAB spray model. A blob injection model similar to that used by Reitz [7] was incorporated. However, in this case the injected blobs were used to represent the intact liquid sheet of the hollow-cone spray instead of the intact liquid core of a high-pressure diesel jet (see Fig. 1). A sheet break-up length was calculated using an expression of Clark and Dombrowski [14]. The inputs, sheet thickness and sheet velocity, were calculated using equations from Lefebvre [15]. Drops within the break-up length were not subject to drag or turbulent dispersion. However, the break-up of the blobs was modeled using the TAB model. When computational results were compared to experimental data, the model of Han et al. [13] was found to predict liquid penetration and SMR satisfactorily. To ensure that the drop size distribution was also similar to experiments, a Rosin-Rammler distribution was assumed upon drop break-up.

In this study, both diesel fuel jets and hollow-cone gasoline sprays are modeled using the KIVA-3v code. Since the sprays of interest are essentially axi-symmetric, a two-dimensional grid is used to keep computer usage time to a minimum. For drop turbulence, drag and evaporation the standard sub-models in KIVA are used [12]. Drop distortion is taken into account by modifying the drag coefficient [16]. This is done using the TAB model, which

compares a drop to a spring-mass system. Drop collision is modeled using the method described in Tennison et al. [17], where an additional "reflexive separation" regime [18] is added to the standard model. Reflexive separation refers to coalescence followed by separation and applies to near head-on droplet collisions. The atomization process uses both the Kelvin-Helmholtz wave model and the Rayleigh-Taylor break-up model. The Rayleigh-Taylor model begins after a specified break-up length and then competes with the Kelvin-Helmholtz break-up already in progress. A discharge coefficient model developed by Sarre et al. [19] is used to take into account the effects of nozzle geometry and ambient conditions on injected drops. Other modifications to the current drop break-up model are also described.

Experiments used for Comparison

Validation of the computational models is performed using three sets of experimental data. The first, and most extensive, is the data collected by Siebers [20]. This data includes liquid penetration measurements as functions of various parameters including ambient temperature, ambient gas density, orifice diameter, fuel temperature, orifice aspect ratio and injection pressure. Table 1 includes a summary of the parameters varied for these runs. The study also includes experimental spray images.

The second experiments are those of Naber and Siebers [21] that provided vapor penetration measurements. These data are valuable for assessing the accuracy of the spray and vaporization models. Table 2 contains a list of the runs from this study that will be used for the vapor penetration comparisons. The table also contains the experimental conditions that are used as inputs for the KIVA calculations.

To validate KIVA predictions of hollow-cone spray behavior, results of Parrish and Farrell [22] are the third set of data used. This data includes photographs, SMR measurements and spray penetrations for three injection pressures. Table 3 contains a summary of the cases and the conditions for this experimental study. Using these experimental data sets allows the different modifications to the break-up model to be compared and contrasted to assess the performance and help improve the current spray sub-models.

Diesel Spray Model

For the atomization of the injected spray the KH-RT hybrid model is used. The Kelvin-Helmholtz wave model and the Rayleigh-Taylor model and their implementations in the KIVA code are described together with the discharge coefficient model of Sarre et al. [19]. The discharge coefficient model predicts the injected velocity, the effective nozzle diameter, and the cone angle of the injected spray given the ambient conditions and the nozzle geometry.

The blob injection model injects liquid drops with a diameter equal to the effective nozzle diameter and the Kelvin-Helmholtz instability is tracked to predict the break-up of the jet [7].

The Kelvin-Helmholtz model postulates that a parent parcel with radius, r, breaks up to form new droplets with radius, r_c, such that

$$r_c = B_0 \Lambda_{KH} \tag{1}$$

where Λ_{KH} is the wavelength corresponding to the KH wave with the maximum growth rate, Ω_{KH}, and B_0 is a constant equal to 0.61. The frequency of the fastest growing wave and its corresponding wavelength are given by

$$\Omega_{KH} = \frac{0.34 + 0.38 We_g^{1.5}}{(1+Z)(1+1.4T^{0.6})} \sqrt{\frac{s}{r_f r^3}} \tag{2}$$

$$\Lambda_{KH} = \frac{9.02r(1+0.45\sqrt{Z})(1+0.4T^{0.7})}{(1+0.865We_g^{1.67})^{0.6}} \tag{3}$$

where the gas Weber number is defined as $We_g=\rho_g U_r^2 r/\sigma$ and the Ohnesorge number, Z, is

$$Z = \frac{\sqrt{We_l}}{\mathrm{Re}_l} \tag{4}$$

U_r is the relative velocity between the liquid drop and the gas, σ is the surface tension, and ρ_g and ρ_f are the gas and fuel densities, respectively. The liquid Weber number is $We_l=\rho_f U_r^2 r/\sigma$ and the liquid Reynolds number is $Re_l=\rho_f U_r r/\mu_f$, where μ_f is the liquid fuel viscosity. Finally, the Taylor number, T, is calculated as

$$T = Z\sqrt{We_g} \tag{5}$$

During break-up, the parent parcel reduces in diameter due to the loss of mass. The rate of change of the radius of the parent parcel is calculated using

$$\frac{dr}{dt} = \frac{r - r_c}{t_{KH}} \tag{6}$$

where τ_{KH} is the break-up time defined by

$$t_{KH} = \frac{3.726B_1 r}{\Omega_{KH}\Lambda_{KH}} \tag{7}$$

The constant B_1 has been given a variety of values between 10 and 60. However, in this study B_1 is set equal to 40 as recommended by Xin et al. [23].

In this study, the KH model is used to predict the initial break-up of the injected "blobs" or the intact liquid core. The Rayleigh-Taylor model is then used in conjunction with the KH model to predict the secondary break-up of the droplets. The RT model predicts instabilities on the surface of the drop that grow until a certain characteristic break-up time when the drop finally breaks-up.

This competing mechanism was introduced by Su et al. [8]. The RT model is also a wave instability where the frequency of the fastest growing wave is given by

$$\Omega_{RT} = \sqrt{\frac{2}{3\sqrt{3s}} \frac{\left[-g_t(r_f - r_a)\right]^{3/2}}{r_f + r_a}} \tag{8}$$

where g is the acceleration in the direction of travel and is defined by $g_t = \vec{g} \cdot \vec{j} + \vec{a} \cdot \vec{j}$, where $\vec{a}$ is the droplet acceleration, and $\vec{j}$ is the unit vector tangent to the droplet trajectory. The corresponding wave number is

$$K_{RT} = \sqrt{\frac{-g_t(r_f - r_a)}{3s}} \tag{9}$$

The wavelength corresponding to the fastest wave growth rate is $2\pi C_{RT}/K_{RT}$ and is compared to the radius of the droplet. If the wavelength is smaller than the droplet diameter, RT waves are assumed to be growing on the surface of the droplet. Once waves begin to grow on the surface of the drop, the wave growth time is tracked. This time is then compared to the break-up time, defined by

$$t_{RT} = \frac{C_t}{\Omega_{RT}} \tag{10}$$

where C_τ is a constant usually equal to unity [23]. If the RT waves have been growing for a time greater than the break-up time, the drop is assumed to break-up. The radii of the new, smaller droplets is calculated using

$$r_c = \frac{pC_{RT}}{K_{RT}} \tag{11}$$

where C_{RT} is another adjustable constant set equal to 0.1 in this study, unless otherwise noted.

Xin et al. [23] introduced the concept of a liquid break-up length to the KH-RT hybrid model. Based on the theory that break-up occurs at a different rate within and beyond the length of this

liquid core, the RT model was introduced such that it only influenced the drops beyond the break-up length. The break-up length is calculated from Levich theory [10] as

$$L_b = C_b d_o \sqrt{\frac{r_f}{r_a}} \tag{12}$$

where C_b is an adjustable constant. If one assumes inviscid flow, and a gas Weber number of infinity (an acceptable assumption due to the high pressures and velocities of diesel jets) the KH equations reduce to a similar expression for break-up length [24]:

$$L_{b,KH} = U_r t_{KH} = \frac{1}{2} B_1 d_o \sqrt{\frac{r_f}{r_a}} \tag{13}$$

In order to keep these two break-up lengths approximately equal to one-another, the constant C_b was chosen such that $C_b=B_1/2$.

The liquid within the intact liquid core is unlikely to be influenced by the RT instability. However, drops outside the liquid core should be affected by the RT break-up since they are decelerated by drag with the ambient gas. Not only are the drops beyond the break-up length influenced by RT waves, but also those drops that are adjacent to the liquid core and within the break-up length. Thus, in the present study when a new drop is created due to KH break-up of a blob in the liquid core, RT waves are allowed to grow on this new drop if the instability conditions satisfy Equation (10).

It is conceivable that some of the new drops are densely packed close to the liquid core of the jet, such that the surrounding gas might not influence the drop. Therefore, to take this into account, the RT break-up time constant, C_τ, was increased to a value of 9.0 within the break-up length to slow down the RT break-up. This is partially justified because, as mentioned previously, Hiroyasu [5] experimentally showed that break-up occurs at a different rate within and beyond the break-up length. Beyond the break-up length C_τ is equal to unity.

The final modification to the implementation of the RT model is based on a study by Han et al. [13]. Han showed that a Rosin-Rammler (RR) distribution applied to newly created child drops improved the drop size distribution predictions. The distribution is defined as

$$h(r) = 1 - \exp\left(-\frac{r}{\bar{r}}\right)^q \tag{14}$$

where h(r) is the fraction of the total volume of the original drop contained in the new drops with a radius less than r, and the number of drops is obtained from mass conservation. The mean radius, $\bar{r}$, is defined by the Rayleigh-Taylor model in Equation (11), and the distribution parameter, q, was set equal to 3.5. Experimental measurements have shown that a wide range of droplets is usually present in sprays. Although his work was applied to hollow-cone sprays, the idea can still be applied to diesel jets. Arcoumanis [25] applied a drop size distribution to the child drops after break-up in a diesel jet and uses the "maximum entropy formalism" to predict the drop size distribution using the conservation equations of mass, momentum and energy. He also states that it is necessary to apply a drop size distribution to drop break-up to more accurately predict the drop sizes within a diesel jet. However, the simpler RR distribution was used here to determine the effects of applying a distribution to drop sizes after break-up.

Hollow-Cone Spray Computational Model

Assuming that a conical liquid sheet exists in a hollow-cone spray near the nozzle, Han [13] used the blob injection model of Reitz and Diwakar [6] and initial SMD was set equal to the sheet thickness. This idea is illustrated clearly in Figure 1. Because the initial drops represent an intact liquid sheet, they are not subject to the effects of drag or turbulent dispersion. Once these

drops have traveled a distance from the nozzle greater than the break-up length, L_b, they are treated as normal drops. This break-up length is defined as

$$L_b = B\left[\frac{\rho_f \sigma \ln(h/h_o) h \cos\theta}{\rho_a^2 U_r^2}\right] \tag{15}$$

where the constant B is set equal to 3, h is the sheet thickness, and θ is the cone angle of the spray. The parameter $\ln(\eta/\eta_o)$ is determined experimentally to be equal to 12.

The sheet velocity, V, is defined by

$$V = K_v\left(\frac{2\Delta P}{\rho_f}\right)^{0.5} \tag{16}$$

where ΔP is the injection pressure, and the velocity coefficient, K_v, is calculated as

$$K_v = C\left(\frac{1-X}{1+X}\right)^{0.5}\frac{1}{\cos\theta} \tag{17}$$

where C=1.1 and the parameter X is defined as the ratio of the nozzle orifice area to the air core area (the area at the nozzle exit filled with an air cone caused by the swirling motion of the spray). Thus, X is defined by

$$X = \left(1-\frac{2h}{d_o}\right)^2 \tag{18}$$

where d_o is the nozzle diameter. The sheet thickness, h, is defined as a function of X, such that

$$h = \left[A\frac{12}{\pi}\frac{\mu_f \dot{m}}{d_o \rho_f \Delta P}\frac{1+X}{(1-X)^2}\right]^{0.5} \tag{19}$$

where A=400, and $\dot{m}$ is the liquid mass flow rate.

The final modification to the TAB model made by Han et al. [10] includes a replacement of the χ^2 distribution, applied to new drops after break-up in KIVA, with a Rosin-Rammler

distribution. This distribution is defined by Equation (14), and better represents experimental drop size distribution measurements than the χ^2 distribution.

In the present study, the KH-RT model is applied to hollow-cone sprays very similar to the way in which it is applied to diesel jets. An intact liquid sheet is assumed to exist near the nozzle with a break-up length defined using Equation (15) from the Han model. The break-up of this liquid sheet is modeled using the KH instability model. Secondary break-up of the drops that have traversed a distance greater than the break-up length is modeled with the competing mechanisms of the RT and KH instabilities. The constants for these two models were optimized such that the model predictions agreed with experimental data. The KH constant, B_1, was set equal to 10. The RT constant C_τ was also set equal to 10. All other constants remained equal to the values used for diesel spray simulations. Drop sizes after RT break-up follow an RR distribution defined by Equation (14) with the distribution parameter, q, equal to 10.0.

The inputs for the model are defined using the same equations as the Han model. The sheet velocity, V, is defined using Equation (16), and the sheet thickness, h, is defined using Equation (19). The blob injection model is again used to define the initial drop sizes, such that the initial SMR is equal to one-half the sheet thickness.

The RT model applies to the break-up of drops in a high-speed gas environment. However, it is of interest to question how the KH model can be used to simulate both the break-up of a diesel jet core and a hollow-cone sheet. This can be explained with an analysis of the general dispersion relations for each spray type.

An analysis of the dispersion relationships for high speed, inviscid jets or sheets shows that for short waves the wave growth rate for a diesel jet is the same as that for a hollow-cone sheet. Senecal et al. [26] came to the same conclusion, stating that “short waves are independent of the

nature of the surface on which they grow." This justifies the use of the KH model for the simulation of both jet and sheet break-up.

Results and Discussion

Results of the present implementations of the spray model are discussed in this section. It was found that the nozzle discharge coefficient model had little to no effect on the liquid penetration or the behavior of the spray since the predicted values were in close agreement with the experimental values used as input originally. The discharge coefficient will be discussed later and compared to experimental data from Siebers [20]. The baseline model used for the comparisons includes the RR distribution, the discharge coefficient model and the added RT break-up with a time constant of C_τ=9.0 (see Equation 10).

Grid Sensitivity Study

The effect of grid sensitivity on spray predictions has been discussed recently by Abraham et al. [27], who concluded hat spray computations may require impractically fine grids. However, the models used in that study and the study of Patterson [28] differ from the present models in several important respects. Firstly, the present model imposes a break-up length region near the nozzle whose length is independent of grid size (it depends only on injection parameters, see Equation 12). Thus, as the grid is refined, the extent of the liquid source region remains fixed in space. This was not the case in the Patterson study, in which a break-up length was not specified but rather an attempt was made to resolve the core region. Secondly, the Abraham model postulates that the liquid is instantaneously broken up into very small drops (e.g., 1-μm diameter) at the nozzle exit, or close to the nozzle. In this case, the injection cell is a point-source singularity of mass and momentum that can cause numerical difficulties near the nozzle exit. In

contrast, the present breakup length and "blob" technique more gradually introduces spray drops into the computational domain. Thus, differences in the grid sensitivity of the various methods are to be expected. In fact, the present spray model was not very sensitive to grid effects.

Figure 2 shows two grids analyzed in this study using the standard approach of grid refinement to assess the influence of grid resolution on the predictions. The finer grid has a cell size of 1×1 mm^2. The courser grid has a cell size of 2×2 mm^2 and was used for all the calculations unless otherwise noted. Both grids are 10 cm wide and 20 cm in length.

Figure 3 shows the effect of grid cell size on the predicted spray tip penetration as a function of ambient gas density for a diesel spray case. The tip penetration was defined by monitoring the location of the 3% liquid volume contour at the leading edge of the spray [24]. The smaller cell size tends to cause longer penetration lengths than the larger grid cell size. This trend was also observed by Patterson [28]. However, in his case the sensitivity to the grid cell size was much more pronounced since that study did not use the breakup length concept. At high ambient densities, there is somewhat less grid sensitivity. This is important, because in engine simulations the gas density is high.

The model constants were optimized in this study to match experimental data. However, this was done using the coarser computational grid. When using the finer grid it is possible to slightly adjust some model constants so that the results match the experimental data better. Two constants can reduce the penetration length at low ambient densities: decreasing the Rosin-Rammler distribution parameter, q, decreases the liquid penetration lengths at low ambient densities. This trend can also be seen in Figure 4. The Rayleigh-Taylor time-constant, C_τ, could also be decreased to adjust the liquid penetration length. This value tends to have a larger effect

on the penetration length at low ambient densities. However, if the constant is decreased too much, the penetration length can increase at low ambient gas temperatures. This trend is shown in Figures 5 and 6.

Effect of the Rosin-Rammler Distribution

Figure 4 shows the liquid penetration as a function of gas density at an ambient temperature of T=850 K. In this plot, the experimental data is compared to the computed data with and without the RR distribution. In general, there is good agreement between the measured and predicted trend. The liquid penetration length decreases significantly at high gas densities. Adding the RR distribution to the child drops tends to increase the predicted liquid penetration, especially at low ambient densities. If the RR distribution parameter is decreased (i.e., the width of the distribution is increased), the penetration length increases more. The explanation for this phenomenon can be found by examining Figure 7.

Figure 7 shows the time-averaged drop size distributions for computed, non-vaporizing sprays with an ambient density of 7.3 kg/m^3 at all radial locations at a distance of 39 mm downstream of the nozzle. The added RR distribution not only increases the range of drop sizes in the spray, but also increases the mean drop size. Since the mean drop size is larger, the spray takes longer to vaporize completely, resulting in a longer liquid penetration length. By increasing the distribution parameter from 3.5 to 5.0, the range and the mean drop size are decreased. Because the experimental data of Siebers [20] does not provide drop size distribution measurements, an optimal distribution parameter could not be determined. A value of 3.5 was used for the distribution parameter in all further calculations since this gave reasonable drop size results.

Effect of Additional RT Break-up

The RT break-up model in this study includes consideration of those drops outside the liquid core but within the break-up length. Figure 5 shows the predicted and measured liquid penetration as a function of temperature at an ambient density of 7.3 kg/m^3. In this plot the experimental data is compared to computations without the additional RT break-up and with the RT break-up using three different time constants (C_τ in Equation 10). Without the RT break-up the model predicts that the penetration has little or no dependence on temperature, which is inconsistent with the measured data. However, with the additional RT break-up the penetration is a strong function of ambient temperature and agrees well with the experimental data. This plot also shows that the model is very sensitive to the time constant, C_τ. If the time constant is too low, the model drastically over-predicts the liquid penetration at low temperatures. This behavior can be explained by examining Figures 6 and 8.

Figure 6 shows images of the sprays for different values of C_τ, at times after the beginning of injection when a pseudo-steady liquid penetration has been reached. The image computed with a time constant of C_τ=9.0 seems to provide the best agreement with experimental images (see also Figure 9). Without the added RT break-up the spray spreads out at first, but does not narrow toward the tip of the spray as the experimental images do. At low values of C_τ small drops evaporate quickly while larger drops coalesce together causing clumps that remain as liquid for a long period of time. When these larger drops finally evaporate, the spray shortens rapidly causing the erratic behavior of the spray tip penetration seen in Figure 8. Figure 8 shows the penetration versus time for two different values of C_τ at an ambient temperature of 850 K and a gas density of 7.3 kg/m^3. The lower break-up constant, C_τ=4.0, causes erratic temporal fluctuations in the liquid penetration length presumably due to clumping coalescence of drops.

The higher value of C_τ=9.0 provides better agreement with the experimental trends [20]. For engine simulations it is important that the transient behavior of the spray is accurately represented.

Liquid Penetration

Figure 9 shows the computed and experimental spray images for a diesel fuel jet at three different conditions. These conditions are the same as those for the experimental images [20]. The shapes of the sprays predicted by the present model are seen to be very similar to the experimental images. In particular, the images at ambient densities of 7.3 kg/m^3 and 14.8 kg/m^3 match extremely well. The sprays spread out gradually as the surrounding gas becomes entrained with the liquid drops. The liquid spray then thins out as the drops begin to evaporate. At an ambient density of 30.2 kg/m^3, the model predicts a slightly wider spray than the one in the experimental image. Also, some small drops remain unevaporated outside the main body of the spray. These drops are due to a vortex cloud that developed at the tip of the jet as the spray was injected into the high-pressure environment. As time progresses, more of these drops evaporate. If enough time were allowed, they would evaporate completely.

The predicted penetration as a function of orifice diameter is compared to experimental data for diesel fuel #2 in Figure 10. The solid lines and symbols represent the computed data and the dashed lines and hollow symbols represent the measured data. The code predicts values fairly close to the experimental data and similar trends. The liquid penetration increases linearly with orifice diameter. At large values of orifice diameter the spray model tends to over-predict the liquid penetration. However, at lower values, the model is more accurate.

Figure 11 compares the experimental penetration lengths as a function of injection pressure to the predicted values. As can be seen, both the trends and the magnitudes agree well with the

experimental data. The liquid penetration is independent of injection pressure in both the experiments and the computations. Once again, at higher values of orifice diameter the computational model over-predicts the penetration length.

Siebers [20] argued that turbulent mixing of the drops and the surrounding gas controls the penetration length or the fuel vaporization. In order for a spray to reach a constant liquid penetration, the rate of vaporization must equal the injected fuel mass flow rate. This means that enough of the air must be entrained into the spray to provide the energy to vaporize the fuel at the same rate at which it is injected. As the spray lengthens, more of the surrounding gas is entrained into the spray. The linear dependence between the penetration and the orifice diameter implies that doubling the orifice diameter would require a liquid length twice as long in order to allow enough air to be entrained into the spray. The lack of dependence on injection pressure implies that higher injection pressures increase the rate of gas entrainment proportionally to accommodate for the increase in the fuel mass flow rate. Because the correct trends are predicted, this implies that in spite of using a low-order moment closure like the k-e model (with its known deficiencies), the turbulence model predicts a consistent amount of gas entrainment. However, because the liquid penetration is over-predicted for large orifice diameters, this implies that not enough air is being entrained into the liquid core for large diameter nozzles. The extent of the KH break-up within the liquid core could be increased to increase the amount of gas entrainment.

Figure 12 shows penetration length as a function of fuel temperature. Once again the predictions of the computational model agree remarkably well with the experimental data. Both sets of data show slightly decreasing penetration lengths with increasing fuel temperature at low ambient temperatures and densities. Based on the mixing controlled vaporization theory of

Siebers [20], the explanation for this trend is obvious. As the fuel temperature is increased, less entrained air is needed to increase the temperature of the fuel to its critical value. The fact that this trend is predicted satisfactorily again implies that the vaporization model is adequate. At more volatile ambient conditions (i.e., higher gas temperatures), the penetration lengths are independent of fuel temperature. This independence of fuel temperature is due to the fact that the high temperatures and pressures of the surrounding gas environment have a large effect on the fuel spray. Thus, the effects of fuel temperature become negligible compared to the effects of the surrounding gas.

Penetration is plotted as a function of ambient temperature Figures 13. This plot also shows the dependence of penetration on gas density. The trends and values predicted are similar to the experimental data. The penetration length decreases with increasing gas density. Sensitivity to gas density also decreases as the density in increased. The lack of sensitivity to the gas density can be explained by two different phenomena. First, the higher density of the gas at high ambient pressures increases the rate of gas entrainment and thus, the energy available for vaporization increases as well. Second, the spray cone angle also increases with increasing gas density. Since the spray is more dispersed, the spray length required for the necessary amount of gas entrainment shortens. The fact that this trend is predicted satisfactorily implies that the model predicts consistently the amount of energy available in the surrounding gases. It also implies that the atomization model predicts satisfactorily the effect of the high-pressure environment on the spray droplets.

The temperature trend in Figure 13 is similar to the gas density trend. The computational model slightly under-predicts the sensitivity of penetration length to the gas temperature. The lack of dependence on temperature could be caused by two different problems. First, it might be

that not enough air is being entrained into the spray for the temperature of the surrounding gases to have an effect on the temperature of the liquid drops. It also could be the evaporation model that is fails to predict the appropriate effect of gas temperature on the liquid fuel drops. The sensitivity to the gas temperature improved dramatically when RT break-up was applied to drops outside the liquid core and within the break-up length. This implies that the added RT break-up helped to increase the amount of gas entrainment, thus increasing the effect of gas temperature. It also implies that the problem does not lie solely with the evaporation model since this model was not changed. The liquid penetration's dependence on the ambient gas temperature is better, but could still use improvement.

Figure 14 shows computed and experimental penetrations as functions of the orifice aspect ratio. The computed and measured data agree satisfactorily well. Both the values and the trends match. The orifice aspect ratio (l/d) is seen to have little to no effect on the liquid penetration. The increase in penetration observed at the highest aspect ratio is due mostly to the effect of the slight increase in nozzle diameter. Thus, the discharge coefficient model predicts the lack of dependence of the discharge coefficient on orifice aspect ratio.

Table 4 lists the different nozzles used by Siebers [20], the experimental discharge coefficient of each nozzle and the discharge coefficient predicted by the discharge coefficient model used in this study. The model predicts values close to the measured values but is not as sensitive to the nozzle diameter or the orifice aspect ratio as the experimental data. The nozzles used by Siebers [20] are all very similar and do not reveal any significant information on nozzle geometry effects.

Vapor Penetration

Spray model constants were optimized to give the best predictions of the liquid penetrations. However, it was necessary to verify that the vapor penetration or the overall penetration length was also correct. The experiments of Naber and Siebers [21] conveniently provided the overall penetration lengths of cases similar to the liquid penetration cases studied in the previous section.

Figure 15 compares the vapor penetration length measurements of Naber and Siebers [21] to the computed penetration length determined from the location of the 5% vapor contour at the spray tip. The present predictions are seen to agree well with the experimental measurements. The model predicts not only the correct lengths, but also the correct rate of penetration (slope). This implies that consistent air-fuel mixing rates are predicted.

Hollow Cone Sprays

Figure 16 shows the experimental spray images and the spray images computed with the previous Han model [13] and with the present KH-RT model. The two models are seen to predict similar but slightly different spray shapes. However, when compared to the experimental images in Figure 16, both seem acceptable. Both models predict the existence of the vortex clouds at the leading edge of the spray.

The drops from the initial slug are more pronounced in the KH-RT model images. This is due to the fact that the KH-RT model produces new parcels when enough drops have been created to fill those parcels. The TAB model used in the Han model does not produce new parcels. So, although the slug appears to contain more mass in the KH-RT model images, the two models predict the same amount of mass in the spray.

The Han model predicts a significant amount of collapse in the cone shape of the spray as time progresses. This phenomenon is also seen clearly in the experimental images. The KH-RT

model also predicts some collapse; however, it is not as pronounced as it should be. The reason for this can be seen in Figure 17. This figure shows the computed gas flow field for the Han and KH-RT models. In both models, the spray motion causes the gas to recirculate through the cone causing it to collapse inward. The recirculation also carries small drops from the tip of the spray causing the vortex cloud. The recirculation predicted by the Han model is more significant than the recirculation predicted by the KH-RT model. Thus, the Han model predicts more cone collapse and a larger vortex cloud. Because the turbulence, drag and collision models are the same for each case, the difference in the gas flow field is caused by the slightly different drop sizes predicted by the different atomization models.

Figure 18 compares experimentally measured tip penetrations to the penetrations predicted by the models. Both the Han model and the KH-RT model show good agreement for all three injection pressure cases [24], however only the 4.76 MPa injection pressure case is shown here.

Figure 19 compares the experimentally measured SMD 39 mm downstream of the nozzle to the predicted SMD values at that location. Both models show fairly good agreement. However, the KH-RT model tends to over-predict drop size and the Han model slightly under-predicts drop size. These differences in drop size are most likely the cause for the different gas flow fields seen in Figure 17. The larger drops predicted by the KH-RT model have more momentum and cause less recirculation in the surrounding gas. Furthermore, the small drops predicted by the Han model are more likely to be affected by the recirculation, creating a larger vortex cloud. The models predict large drop sizes at first and fairly constant drop sizes later in time.

The predicted drop size distributions are compared to the experimental drop size distribution in Figure 20. The experimental results show a wider range of drop sizes than is predicted by the computations. The Han model predicts less numerous small and large drops and more drops of

average size. The KH-RT model predicts even more averaged-size drops. However, the mean drop size of both models agrees with the measured data. This prediction agrees with the trends shown in Figure 19.

Summary and Conclusions

This study focused on the analysis and improvement of spray atomization models for use in multi-dimensional modeling. The KH-RT hybrid model was used to model both diesel jets and hollow-cone sprays. The implementation of the Rayleigh-Taylor break-up model was changed such that all drops outside a liquid core region near the nozzle exit were subject to RT accelerative instabilities. Also, a Rosin-Rammler distribution was used to define the children drop sizes after the RT break-up of a parent parcel. A discharge coefficient model was incorporated to predict the initial behavior of the injected spray, given the nozzle geometry and the ambient conditions inside the spray bomb. The results from the computations were compared to three sets of experimental data [16,17, and18]. The model's predictions of hollow-cone spray behavior were also compared to the computational results obtained using a previous model [10].

The new computational model was found to satisfactorily predict the trends and values of the diesel jet experimental measurements. In particular, the additional RT break-up improved the temperature dependence of the liquid penetration significantly due to its effect on air entrainment. The Rosin-Rammler distribution was found to increase the range of drop sizes in the spray and tended to increase the liquid penetration at low ambient densities.

The predictions of hollow-cone spray behavior also agreed well with the experimental data. In terms of the values of the model constants, the values of B_0, B_1, C_{RT}, and C_b were not changed

from diesel to gasoline sprays. The constants, C_{RT} and C_b are related. Thus, only 3 constants: C_{RT}, C_τ, and q were available for change, and of these, only C_τ and q are changed between gasoline and Diesel sprays. Since the experimental data-base matched is very extensive it is felt that that the present model should be useful in diverse modeling applications. Based on the present study, it is concluded that the present KH-RT model would useful in engine simulations. The use of one model to predict both diesel jet behavior and hollow-cone spray behavior will simplify atomization sub-models and improve confidence in multi-dimensional modeling.

Acknowledgements

Ford Motor Co., the Army Research Office, Caterpillar, and DOE/Sandia Laboratories provided financial support for this work. The authors thank Chris Sarre, Song-Charng Kong, Allen Han, Rick Anderson, Dennis Siebers, Sudakar Das, and Kelly Senecal for their help.

References

1. P. Pelloni and G. M. Bianchi, Modeling the Diesel Fuel Spray Break-up by Using a Hybrid Model. SAE Technical Paper 1999-01-0226, Society of Automotive Engineers, Warrendale, PA, 1999.
2. M. A. Patterson and R. D. Reitz, Modeling the effects of Fuel Spray Characteristics on Diesel Engine Combustion and Emissions. SAE Technical Paper 980131, Society of Automotive Engineers, Warrendale, PA, 1998.
3. R. D. Reitz and F. V. Bracco, Mechanism of Atomization of a Liquid Jet. *Phys. Fluids*, vol. 25, pp. 1730 – 1742, American Institute of Physics, 1982.
4. H. Hiroyasu, M. Arai and M. Shimizu, Break-up Length of a Liquid Jet and Internal Flow in a Nozzle. ICLASS-91, Gaithersburg, MD, U.S.A., July 1991.
5. F.V. Bracco, Modeling of Engine Sprays, SAE Trans., Vol. 94, pp. 144-167, 1985.
6. R. D. Reitz and R. Diwakar, Structure of High-pressure Fuel Sprays. SAE Technical Paper 870598, Society of Automotive Engineers, Warrendale, PA, 1987.
7. R. D. Reitz, Modeling Atomization Processes in High-pressure Vaporizing Sprays. *Atomization and Spray Technology*, vol. 3, pp. 309-337, 1987.
8. T. F. Su, M. A. Patterson, R. D. Reitz and P. V. Farrell, Experimental and Numerical Studies of High Pressure Multiple Injection Sprays. SAE Technical Paper 960861, Society of Automotive Engineers, Warrendale, PA, 1996.
9. L. M. Ricart, J. Xin, G. R. Bower and R. D. Reitz, In-Cylinder Measurement and Modeling of Liquid Fuel Spray Penetration in a Heavy-duty Diesel Engine. SAE Technical Paper 971591, Society of Automotive Engineers, Warrendale, PA, 1997.
10. V. G. Levich, *Physicochemical Hydrodynamics*. Prentice-Hall, New Jersey, 1962.

11. P. J. O'Rourke and A. A. Amsden, The Tab Method for Numerical Calculation of Spray Droplet Break-up. SAE Technical Paper 872089, Society of Automotive Engineers, Warrendale, PA, 1987.
12. Amsden, A. A., O'Rourke, P. J. and Butler, T. D., "KIVA-II: A Computer Program for Chemically Reactive Flows with Sprays," Los Alamos National Laboratory, LA-11560-MS, 1989.
13. Z. Han, S. Parrish, P. V. Farrell and R. D. Reitz, Modeling Atomization Processes of Pressure-Swirl Hollow-Cone Fuel Sprays. *Atomization and Sprays*, vol. 7, pp. 663-684, 1997.
14. P. J. Clark and N. Dombrowski, Aerodynamic Instability and Disintegration of Inviscid Liquid Sheets. *Proc. Roy. Soc. Lond. A*, vol. 329, p. 467, 1972.
15. A. H. Lefebvre, *Atomization and Sprays*, Hemisphere Publishing Corp., New York, 1989.
16. A. B. Liu, D. Mather and R. D. Reitz, Modeling the Effects of Drop Drag and Break-up on Fuel Sprays. SAE Technical Paper 930072, Society of Automotive Engineers, Warrendale, PA, 1993.
17. P. J. Tennison, T. L. Georjon, P. V. Farrell and R. D. Reitz, Experimental and Numerical Study of Sprays from a Common Rail Injection System for Use in an HSDI Diesel Engine. SAE Technical Paper 980346, Society of Automotive Engineers, Warrendale, PA, 1998.
18. N. Ashgriz and J. Y. Poo, Coalescence and Separation in Binary Collisions of Liquid Drops. *J. Fluid Mech*., vol.221, pp.183-204, 1990.
19. C. Sarre, S. Kong and R. D. Reitz, Modeling the Effects of Injector Nozzle Geometry on Diesel Sprays. Submitted to SAE for publication, 1999.

20. J. D. Naber and D. L. Siebers, Effects of Gas Density and Vaporization on Penetration and Dispersion of Diesel Sprays. SAE Technical Paper 960034, Society of Automotive Engineers, Warrendale, PA, 1996.
21. D. L. Siebers, Liquid-Phase Fuel Penetration in Diesel Sprays. SAE Technical Paper 980809, Society of Automotive Engineers, Warrendale, PA, 1998.
22. S. E. Parrish and P. V. Farrell, Transient Spray Characteristics of a Direct-Injection Spark-Ignition Fuel Injector. SAE Technical Paper 970629, Society of Automotive Engineers, Warrendale, PA, 1997.
23. J. Xin, L. Ricart and R. D. Reitz, Computer Modeling of Diesel Spray Atomization and Combustion. *Combustion Science and Technology*, Vol. 137, 1-6, p. 171, 1998.
24. J. C. Beale, Modeling Fuel Injection Using the Kelvin-Helmholtz / Rayleigh-Taylor Hybrid Atomization Model in KIVA-3v, M. S. Thesis, University of Wisconsin, Madison, WI, 1999.
25. C. Arcoumanis and M. Gavaises, Effect of Fuel Injection Processes on the Structure of Diesel Sprays. SAE Technical Paper 970799, Society of Automotive Engineers, Warrendale, PA, 1997.
26. P. K. Senecal, D. P. Schmidt, I. Nouar, C. J. Rutland and R. D. Reitz, Modeling High Speed Viscous Liquid Sheet Atomization. Submitted to SAE for publication, 1999.
27. J. Abraham, What is the Adequate Resolution in the Numerical Computation of Transient Jets? SAE Technical Paper 970051, Society of Automotive Engineers, Warrendale, PA, 1997.
28. M. A. Patterson, Modeling the Effects of Fuel Injection Characteristics on Diesel Combustion and Emissions, Ph. D. Thesis, University of Wisconsin, Madison, WI, 1997.

Table 1: Summary of parameters varied in Siebers [20]

Fuels	Cetane, Diesel Fuel #2
Ambient Gas Density (kg/m^3)	3.6, 7.3, 14.8, 30.2, 59
Ambient Gas Temperature (K)	700, 850, 1000, 1300
Injection Pressure (MPa)	50, 135, 150
Orifice Diameter (μm)	100, 246, 498
Orifice Aspect Ratio	2, 4, 8
Fuel Temperature (K)	375, 400, 425, 450

Table 2: Experimental Runs of Naber and Siebers [21]

Fuel	Diesel Fuel #2
Orifice Diameter	0.257 mm
Injection Pressure	137 MPa
Ambient Gas Temperature	1000 K
Ambient Gas Density	3.3, 6.8, 13.9, 28.6, and 58.6 kg/m^3

Table 3: Experimental runs of Parrish and Farrell [22]

Working Fluid	Stoddard solvent
Volume of Fluid Injected	56.8 cm^3
Injection Duration	3.76 ms
Ambient Air Temperature	300 K
Ambient Air Pressure	1 atm
Nozzle Diameter	0.560 mm
Spray Cone Angle	45° with 10° dispersion angle
Injection Pressure	3.4, 4.76, and 6.12 MPa

Table 4: Measured and Computed Discharge Coefficients

d_o *(mm)*	l/d	$C_{d,\ meas}$	$C_{d,\ calc}$
0.100	4.0	0.80	0.79
0.251	2.2	0.79	0.78
0.246	4.2	0.78	0.79
0.267	8.0	0.77	0.78
0.498	4.3	0.84	0.79

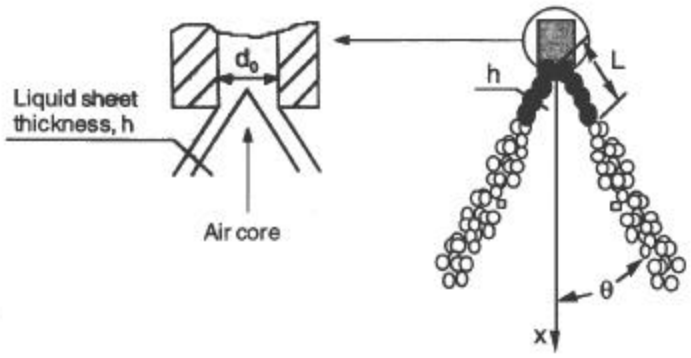

a.)

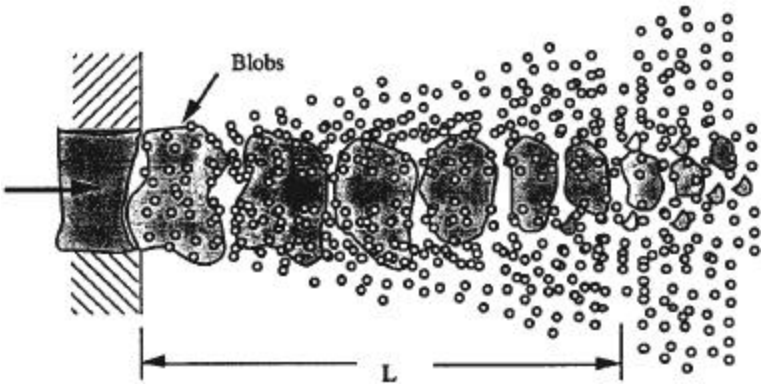

b.)

Figure 1: Schematic showing the conceptual liquid flow structure at the nozzle exit for a.) the sheet break-up processes [10] and, b.) for diesel-type sprays.

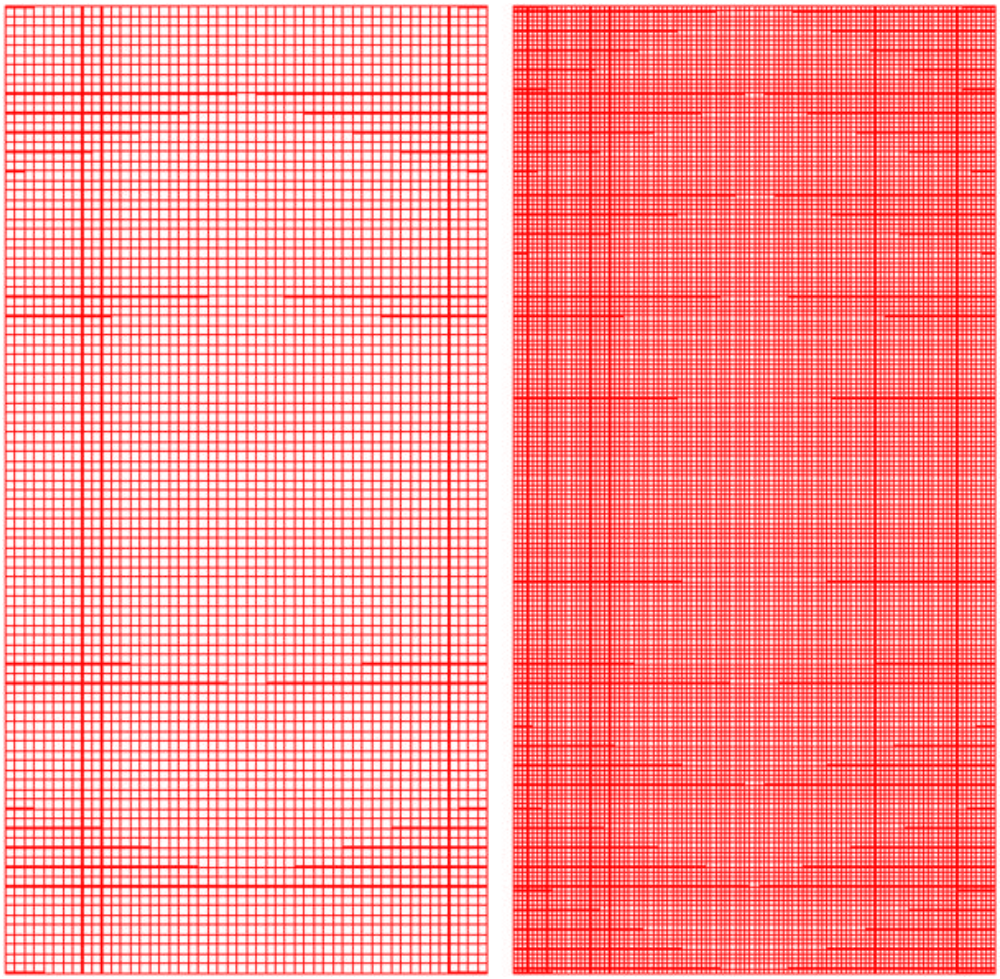

Figure 2: Computational grids. The right and left images are the 2×2-mm grid and the 1×1-mm grid, respectively. Both grids are 10 cm wide and 20 cm in length.

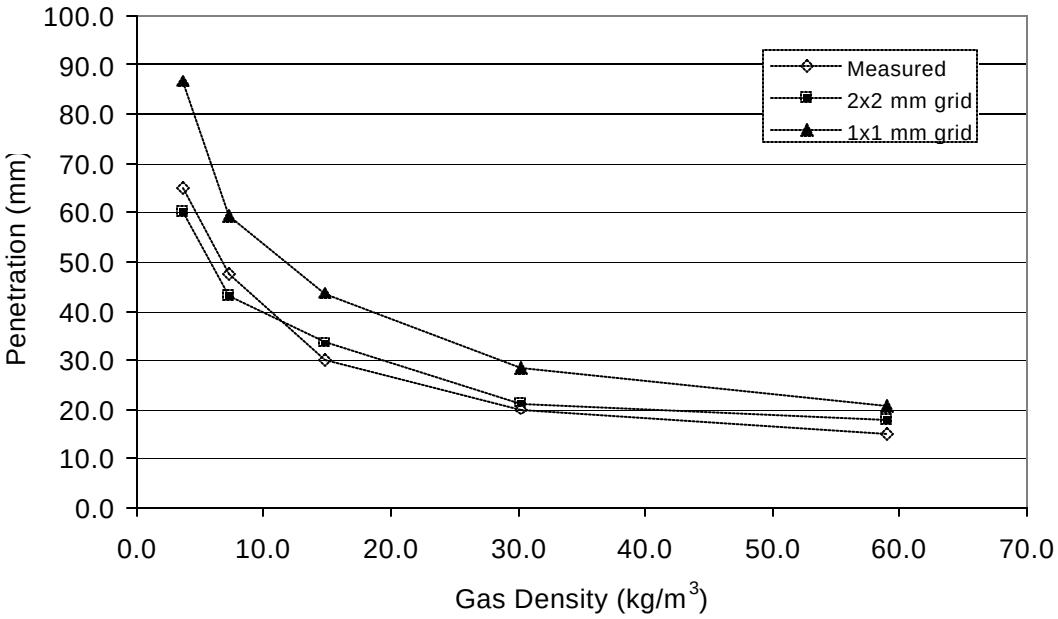

Figure 3: Effect of grid cell size on penetration as a function of gas density. The fuel, gas temperature, injection pressure, and orifice diameter are cetane, 1000 K, 136 MPa, and 246 μm, respectively.

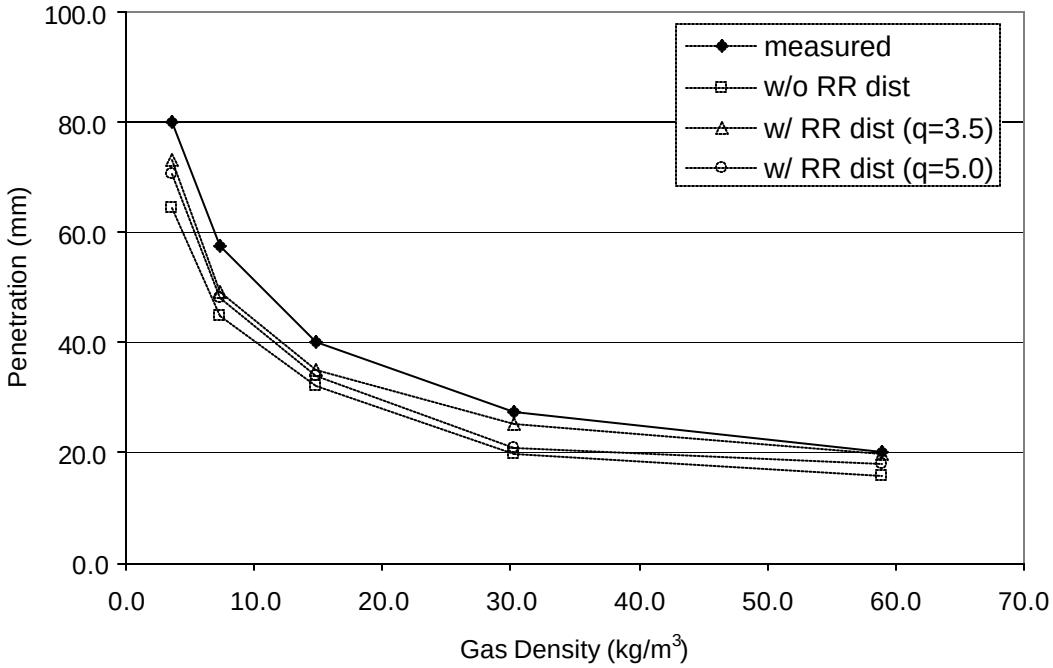

Figure 4: Effect of RR distribution on liquid penetration length as a function of gas density. The fuel, gas temperature, and orifice diameter are cetane, 850 K, and 246 μm, respectively.

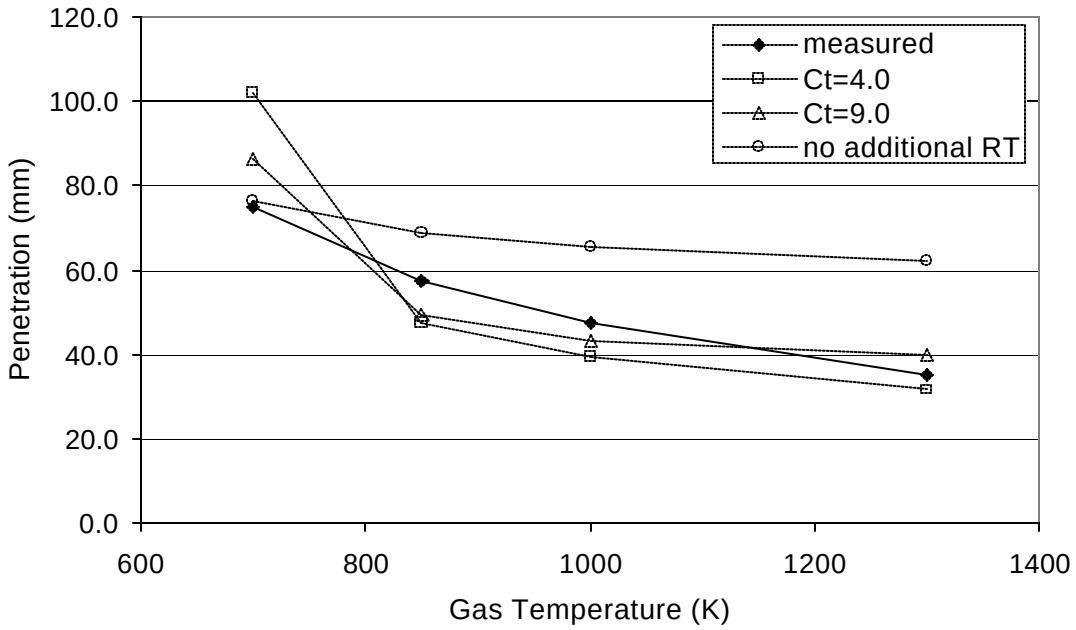

Figure 5: Effect of additional RT break-up on liquid penetration versus gas temperature. The fuel, gas density and orifice diameter are cetane, 7.3 kg/m^3, and 246 μm, respectively.

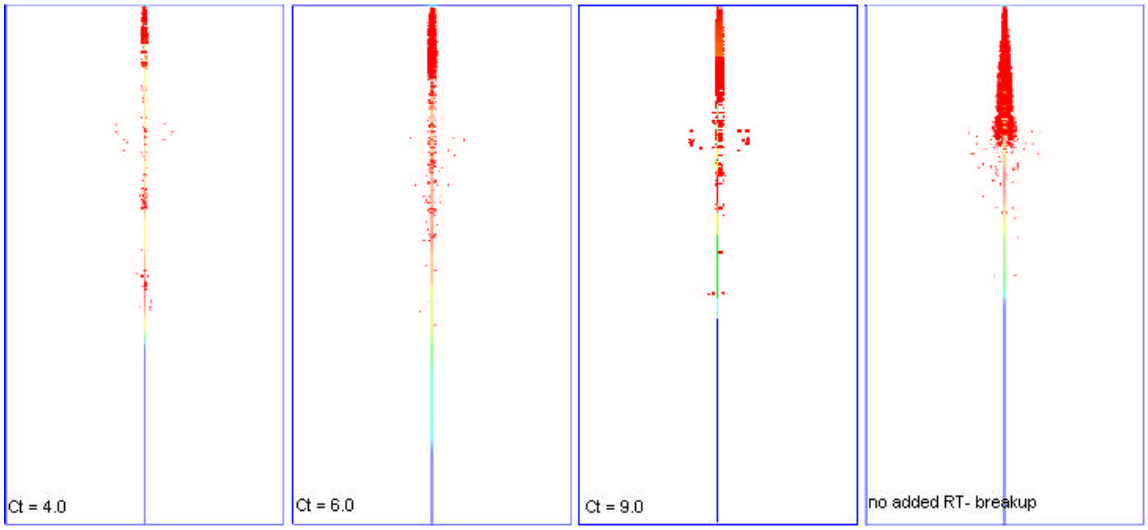

Figure 6: Effect of additional RT break-up on spray shape. The fuel, gas temperature, gas density and orifice diameter are cetane, 700 K, 7.3 kg/m^3, and 246 μm, respectively.

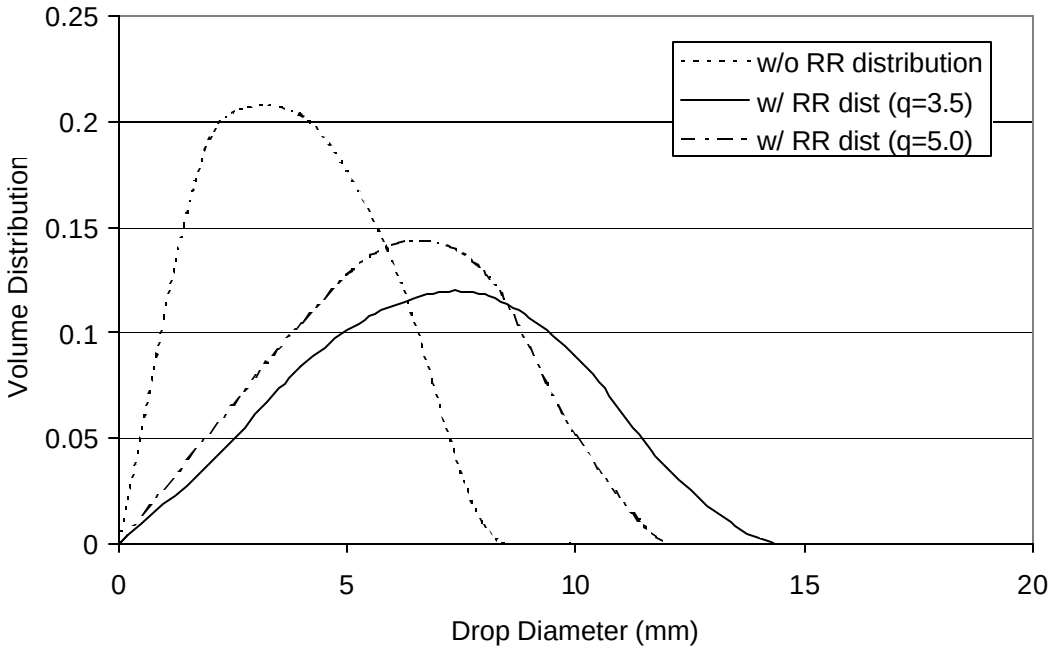

Figure 7: Effect of Rosin-Rammler distribution on time-averaged drop size distribution. The fuel, gas density and orifice diameter are cetane, 7.3 kg/m^3, and 246 μm. The cases are non-vaporizing.

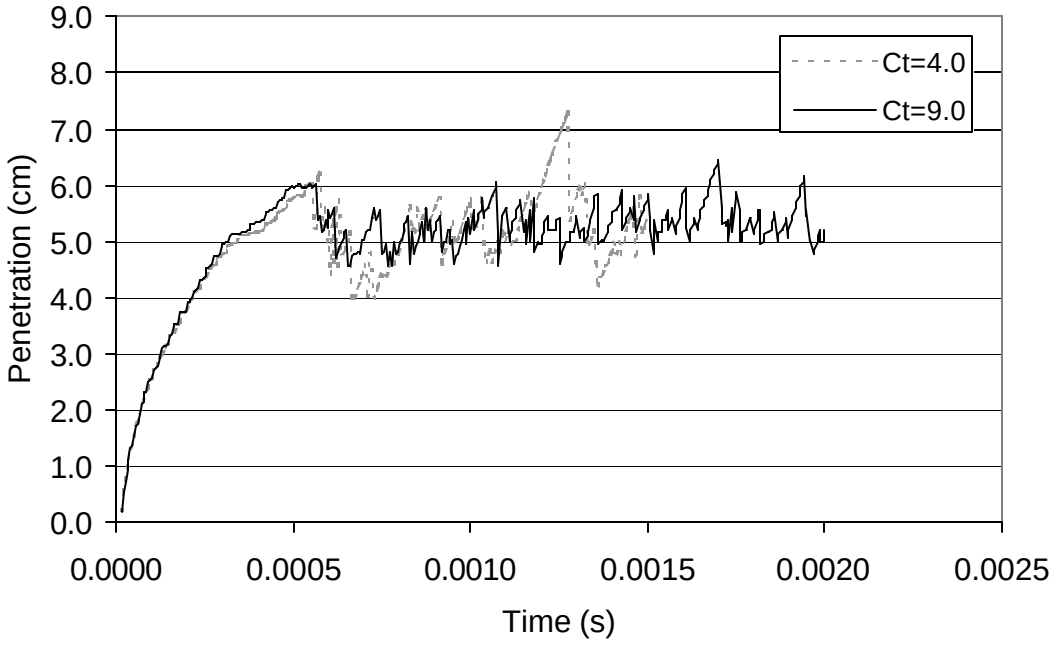

Figure 8: Effect of break-up time constant on penetration as a function of time. The fuel, gas temperature, gas density and orifice diameter are cetane, 850 K, 7.3 kg/m^3, and 246 μm, respectively.

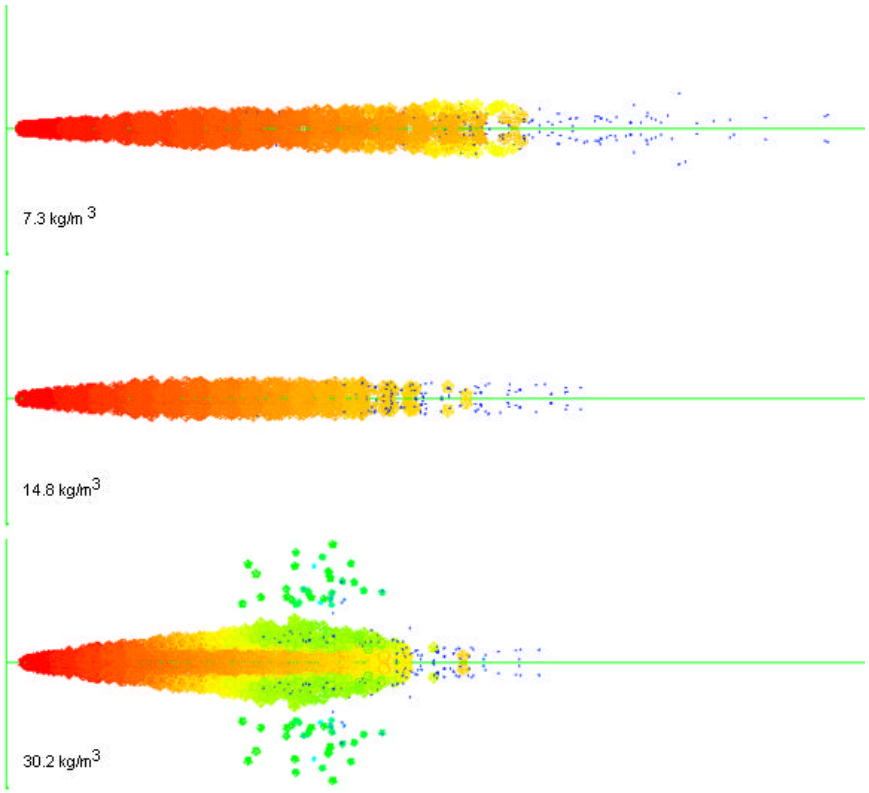

Figure 9: Experimental spray images [20] (top) and computed spray images (bottom). The fuel, gas temperature, injection pressure, and orifice diameter are DF2, 1000 K, 135MPa, and 246 μm, respectively. Drop size is proportional to circle size in the image.

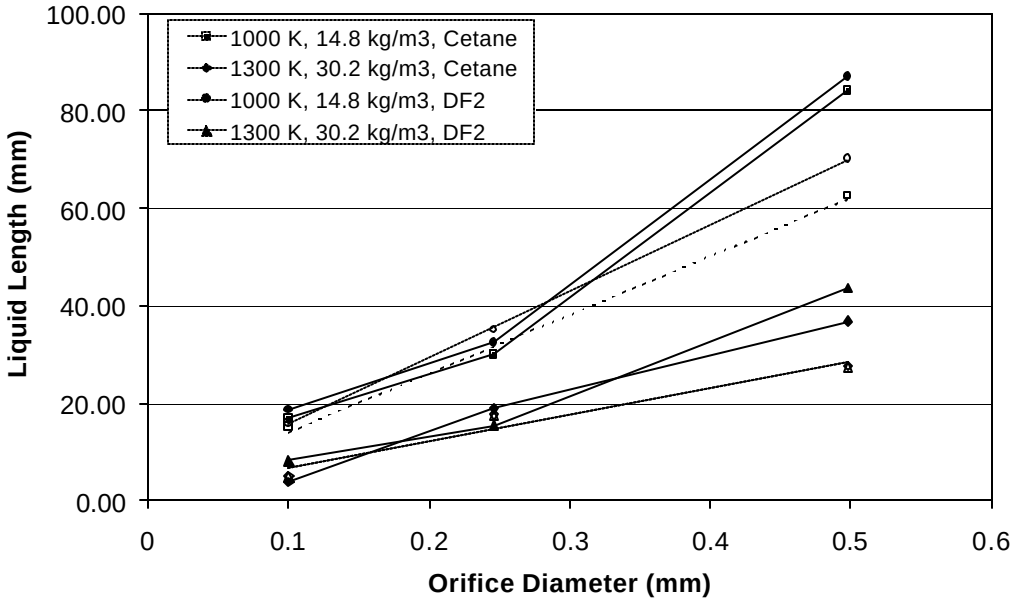

Figure 10: Penetration as a function of orifice diameter. The values in the legend are ambient temperature, ambient gas density, and fuel. The injection pressure is 135 MPa. The solid and dashed lines represent the computed and measured data, respectively.

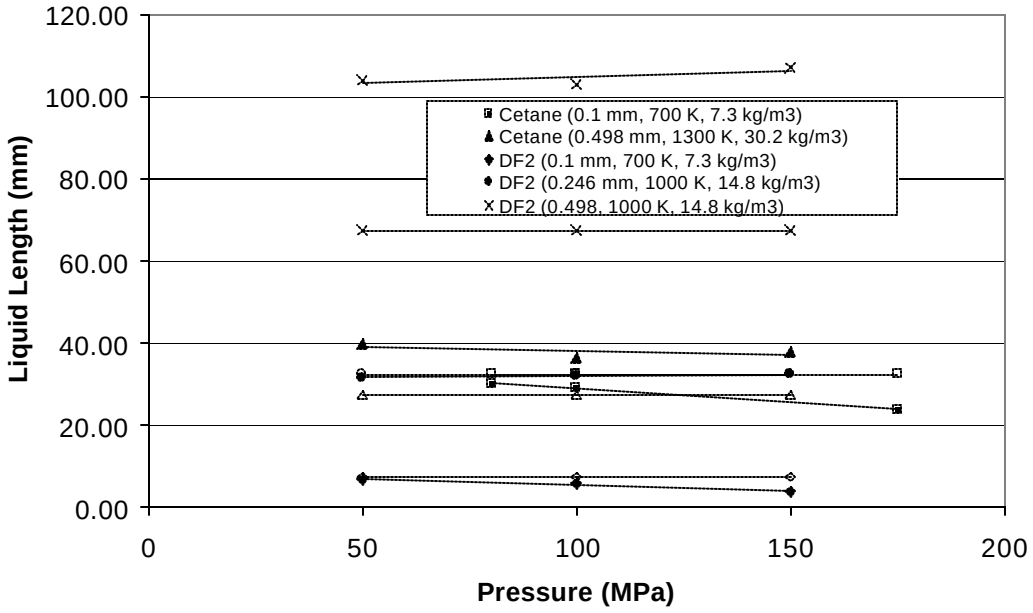

Figure 11: Penetration as a function of injection pressure. The values in the legend include fuel, orifice diameter, ambient temperature, and ambient gas density. The solid and dashed lines represent the computed and measured data, respectively.

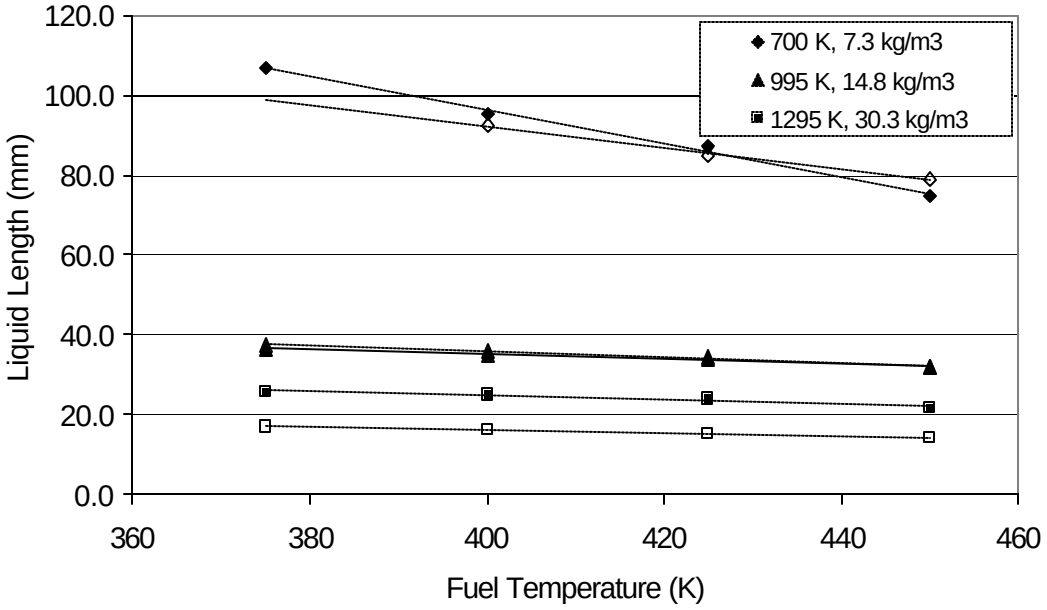

Figure 12: Liquid Penetration as a function of fuel temperature. The values in the legend include ambient temperature and gas density. The orifice diameter and injection pressure are 246 μm and 135 MPa, respectively. The solid and dashed lines represent the computed and measured data, respectively.

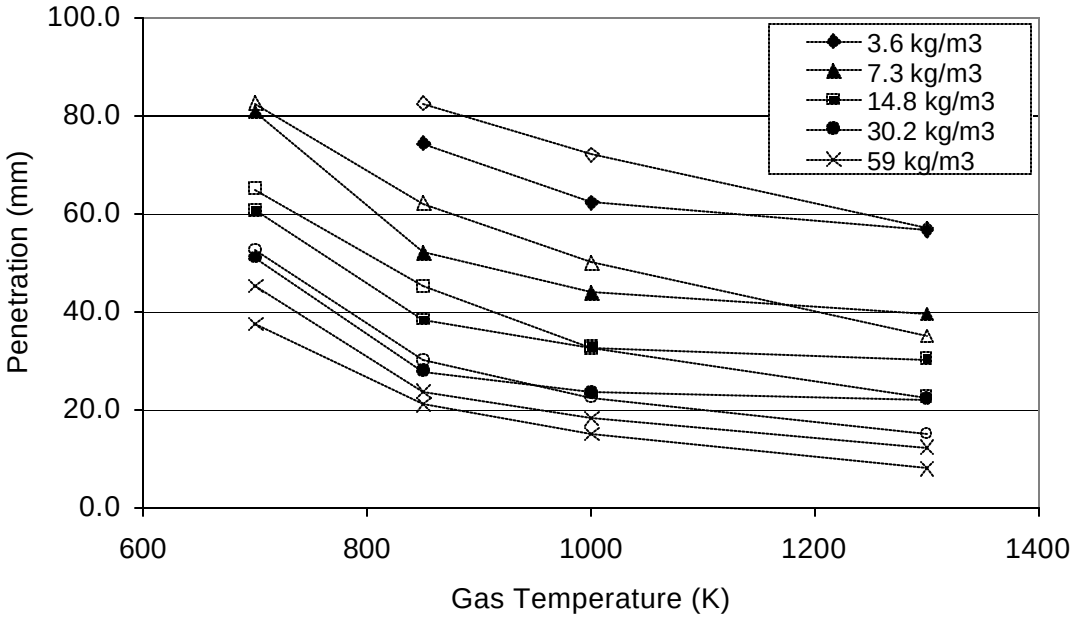

Figure 13: Liquid Penetration as a function of gas temperature. Figures (a) and (b) contain results for cetane and DF2, respectively. The values in the legends are gas density. The injection pressure and the orifice diameter are 135 MPa, and 246 μm, respectively. The solid and dashed lines represent the computed and measured data, respectively.

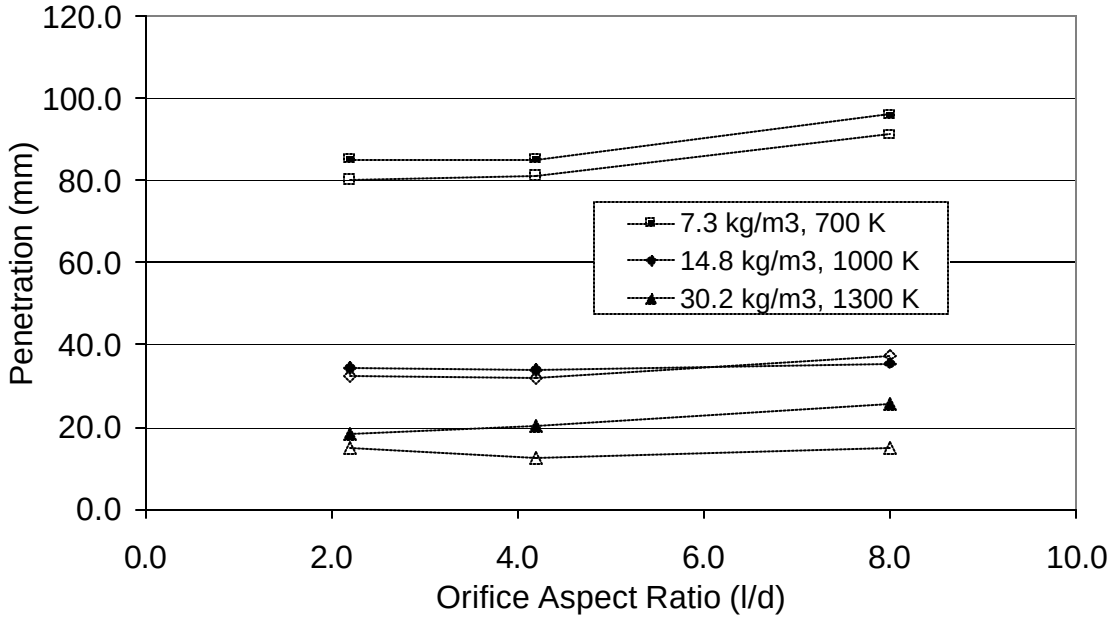

Figure 14: Liquid Penetration as a function of orifice aspect ratio. The values in the legend include ambient gas density and ambient temperature. The fuel, injection pressure, and orifice diameter are DF2, 135 MPa and 246 μm, respectively. The solid and dashed lines represent the computed and measured data, respectively.

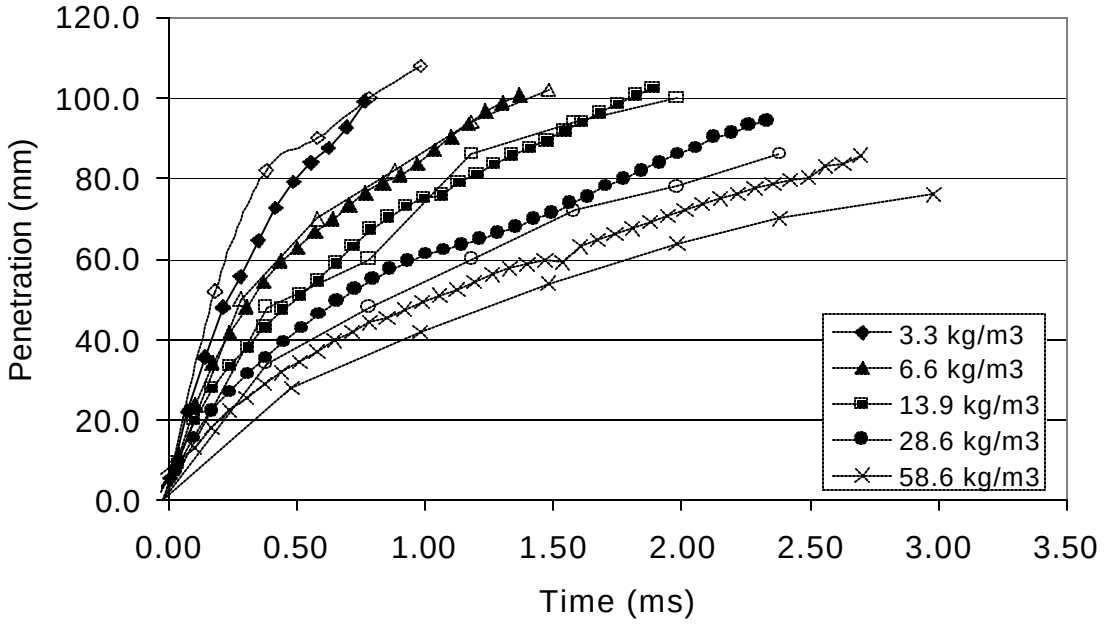

Figure 15: Overall spray penetration as a function of time. The values in the legend are the ambient gas density. All other conditions are listed in Table 2.

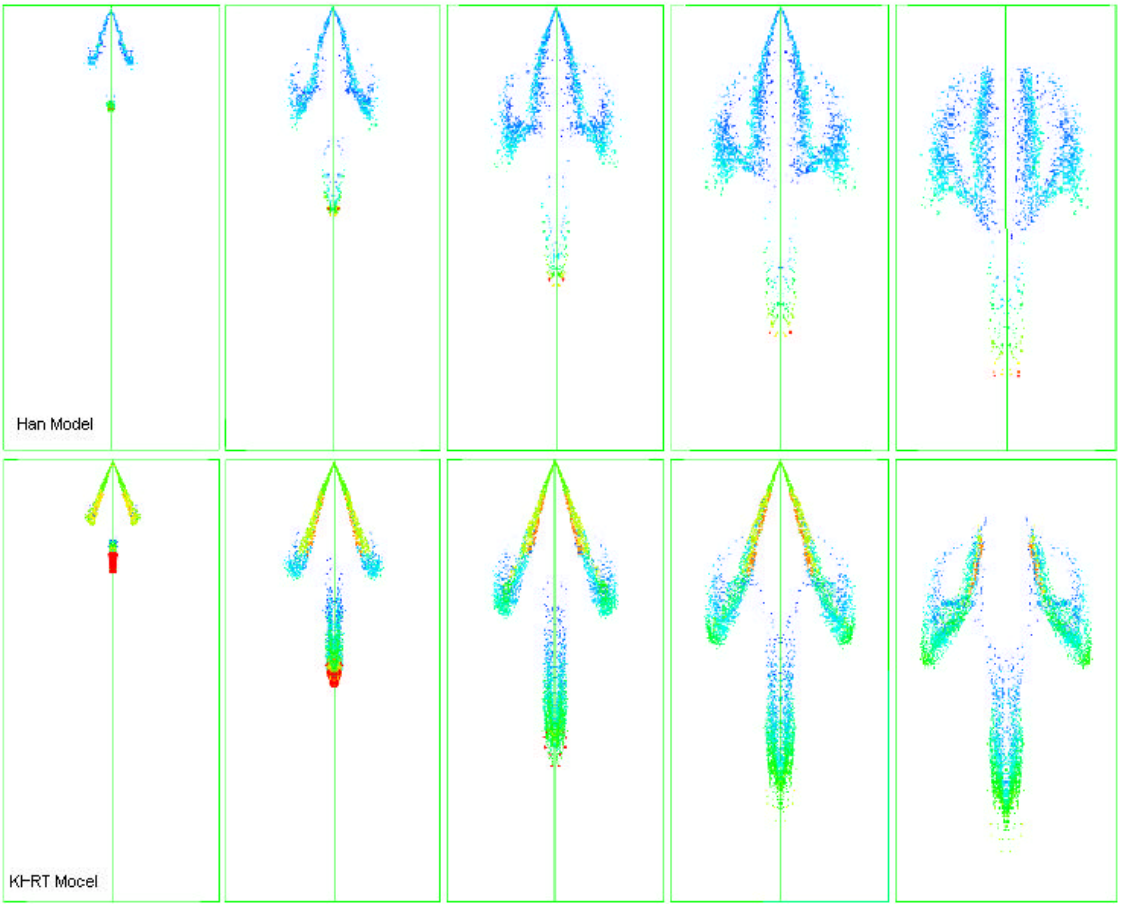

Figure 16: Experimental images [22] (top) and cross-sectional spray images computed using the Han model [13] (middle) and the KH-RT model (bottom) for ΔP=4.76 MPa.

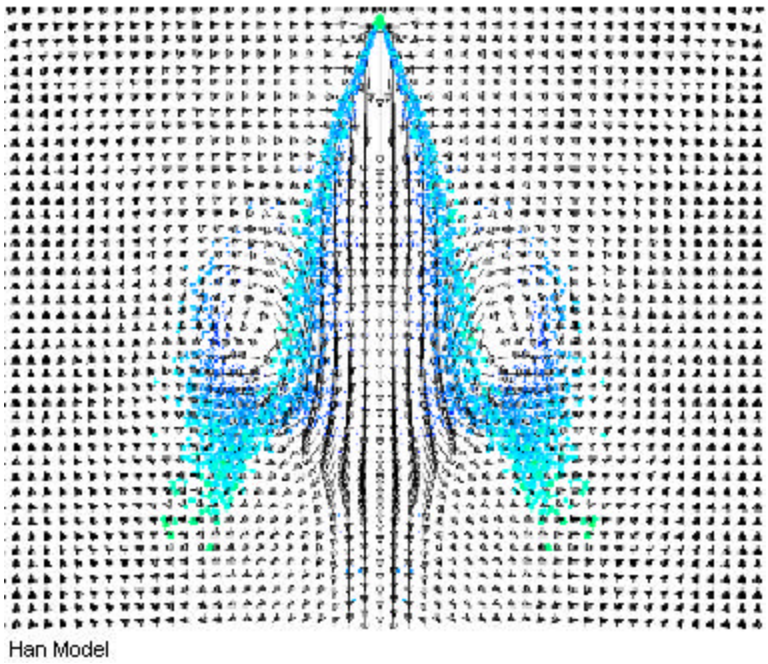

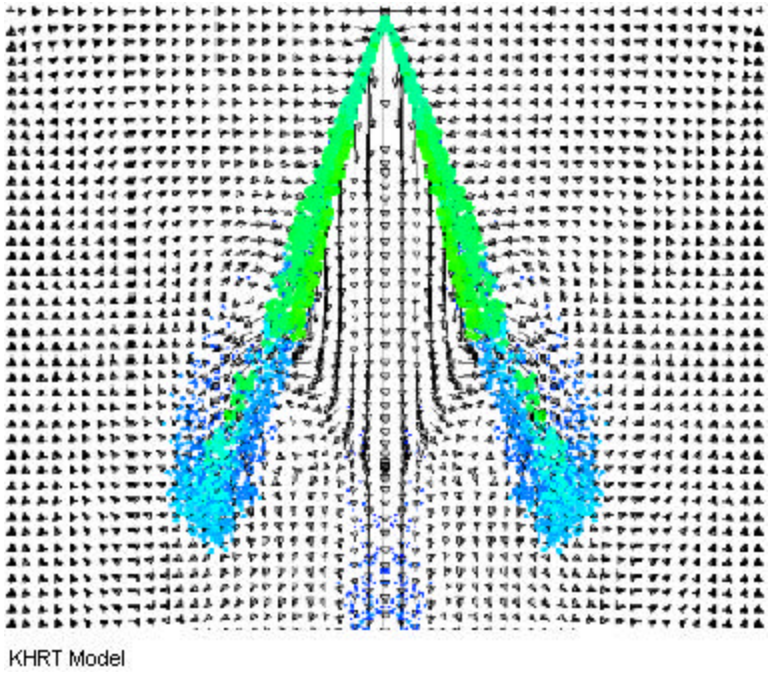

Figure 17: Computed spray-induced gas entrainment superimposed over the computed spray images for ΔP=4.76 MPa.

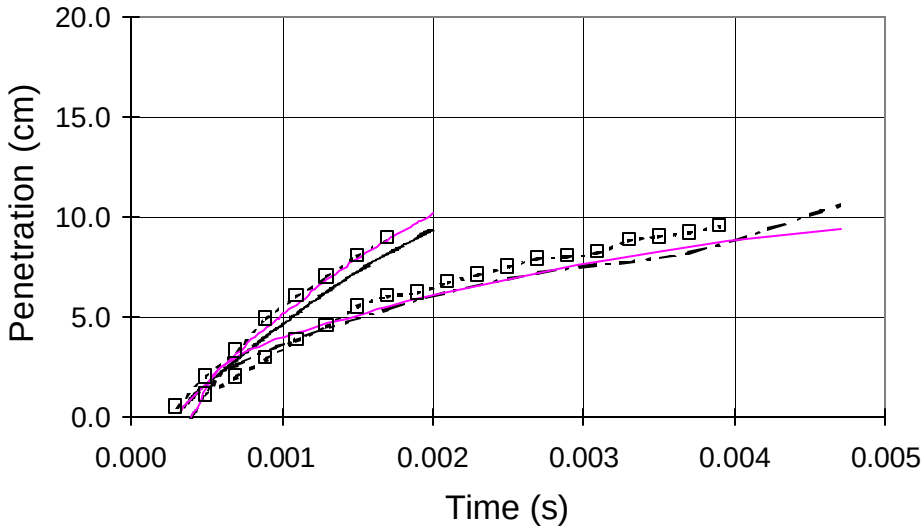

Figure 18: Spray tip penetration as a function of time with injection pressure of 4.76 MPa (Symbols: measured, Solid line: Present KH-RT model, Dashed line: Han Model)

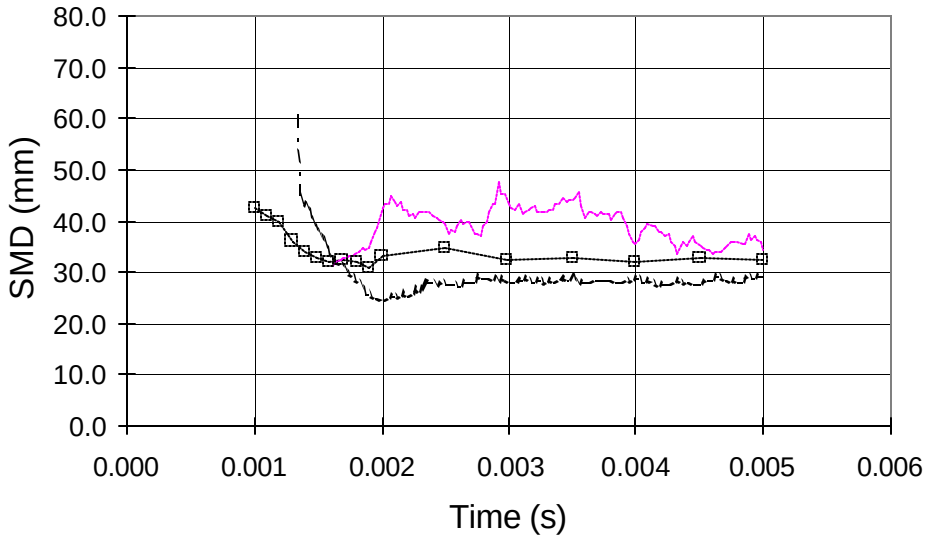

Figure 19: Local Sauter mean diameter as a function of time for injection pressure 4.76 MPa (Symbols: measured, Solid line: Present KH-RT model, Dashed line: Han Model).

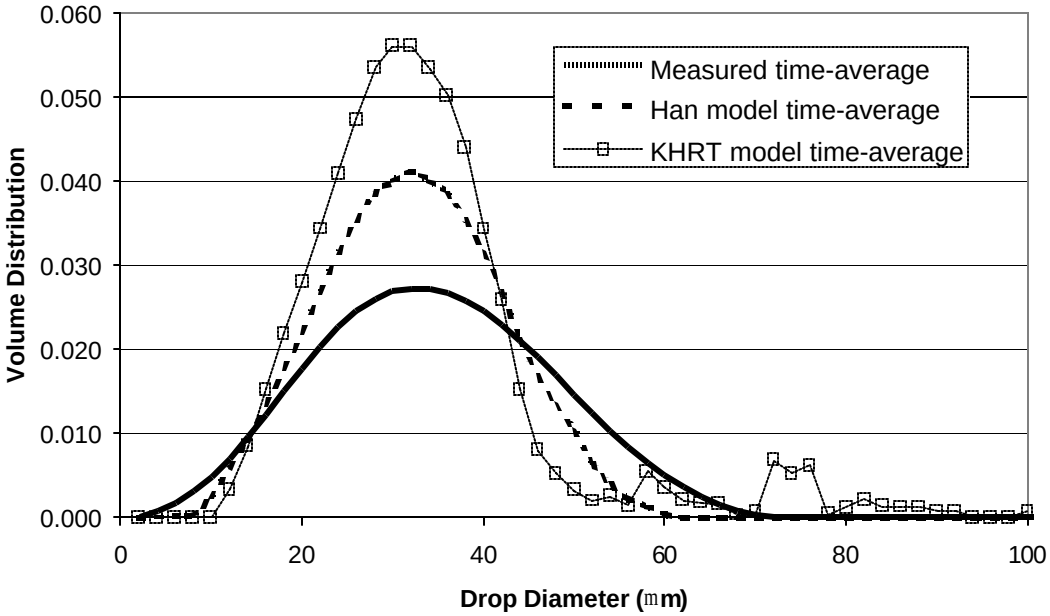

Figure 20: Comparison of measured and computed local drop size distribution for ΔP=4.76 MPa.

Figure 1: Schematic showing the conceptual liquid flow structure at the nozzle exit and the sheet break-up processes [10].

Figure 2: Computational grids. The right and left images are the 2×2-mm grid and the 1×1-mm grid, respectively. Both grids are 10 cm wide and 20 cm in length.

Figure 3: Effect of grid cell size on penetration as a function of gas density. The fuel, gas temperature, injection pressure, and orifice diameter are cetane, 1000 K, 136 MPa, and 246 μm, respectively.

Figure 4: Effect of RR distribution on liquid penetration length as a function of gas density. The fuel, gas temperature, and orifice diameter are cetane, 850 K, and 246 μm, respectively.

Figure 5: Effect of additional RT break-up on liquid penetration versus gas temperature. The fuel, gas density and orifice diameter are cetane, 7.3 kg/m^3, and 246 μm, respectively.

Figure 6: Effect of additional RT break-up on spray shape. The fuel, gas temperature, gas density and orifice diameter are cetane, 700 K, 7.3 kg/m^3, and 246 μm, respectively.

Figure 7: Effect of Rosin-Rammler distribution on time-averaged drop size distribution. The fuel, gas density and orifice diameter are cetane, 7.3 kg/m^3, and 246 μm. The cases are non-vaporizing.

Figure 8: Effect of break-up time constant on penetration as a function of time. The fuel, gas temperature, gas density and orifice diameter are cetane, 850 K, 7.3 kg/m^3, and 246 μm, respectively.

Figure 9: Experimental spray images [20] (top) and computed spray images (bottom). The fuel, gas temperature, injection pressure, and orifice diameter are DF2, 1000 K, 135MPa, and 246 μm, respectively. Drop size is proportional to circle size in the image.

Figure 10: Penetration as a function of orifice diameter. The values in the legend are ambient temperature, ambient gas density, and fuel. The injection pressure is 135 MPa. The solid and dashed lines represent the computed and measured data, respectively.

Figure 11: Penetration as a function of injection pressure. The values in the legend include fuel, orifice diameter, ambient temperature, and ambient gas density. The solid and dashed lines represent the computed and measured data, respectively.

Figure 12: Liquid Penetration as a function of fuel temperature. The values in the legend include ambient temperature and gas density. The orifice diameter and injection pressure are 246 μm and 135 MPa, respectively. The solid and dashed lines represent the computed and measured data, respectively.

Figure 13: Liquid Penetration as a function of gas temperature. Figures (a) and (b) contain results for cetane and DF2, respectively. The values in the legends are gas density. The injection pressure and the orifice diameter are 135 MPa, and 246 μm, respectively. The solid and dashed lines represent the computed and measured data, respectively.

Figure 14: Liquid Penetration as a function of orifice aspect ratio. The values in the legend include ambient gas density and ambient temperature. The fuel, injection

pressure, and orifice diameter are DF2, 135 MPa and 246 μm, respectively. The solid and dashed lines represent the computed and measured data, respectively.

Figure 15: Overall spray penetration as a function of time. The values in the legend are the ambient gas density. All other conditions are listed in Table 2.

Figure 16: Experimental images [22] (top) and cross-sectional spray images computed using the Han model [13] (middle) and the KH-RT model (bottom) for ΔP=4.76 MPa.

Figure 17: Computed spray-induced gas entrainment superimposed over the computed spray images for ΔP=4.76 MPa.

Figure 18: Spray tip penetration as a function of time.

Figure 19: Local sauter mean diameter as a function of time.

Figure 20: Comparison of measured and computed local drop size distribution for ΔP=4.76 MPa.

Nomenclature

$\vec{a}$	Droplet acceleration
A	Han model parameter (= 400)
B	Mass transfer number (= 3)
B_0	Kelvin-Helmholtz model constant (= 0.61)
B_1	Kelvin-Helmholtz model time constant (= 40)
C_b	Break-up constant (= 20)
C_{RT}	Rayleigh-Taylor model size constant (= 0.1)
C_τ	Rayleigh-Taylor model time constant
d_o	Nozzle diameter
g	Gravitational acceleration
g_t	Drop acceleration in direction of travel
h	Hollow cone spray sheet thickness
h(r)	Fraction of total volume of original drop contained in new drops with radii less than r
j	Unit vector tangent to drop trajectory
K_{RT}	Rayleigh-Taylor wave number corresponding to the fastest growing wave
K_v	Han model velocity coefficient
L_b	Break-up length
l/d	Nozzle length to diameter ratio
$\dot{m}$	Fuel mass flow rate
q	Rosin-Rammler distribution parameter (= 3.5)
r	Drop radius
$\bar{r}$	Mean drop radius

r_c	child drop radius after KH or RT break-up
Re	Reynold's number
T	Taylor number
U_r	Relative drop/gas velocity
V	Hollow cone sheet velocity
We	Weber number
X	Han model parameter
Z	Ohnesorge number
ΔP	Injection pressure
θ	Spray cone angle
Λ_{KH}	Wavelength corresponding to maximum KH wave growth rate
μ	Air viscosity
ρ	density
σ	Surface tension
τ	break-up time
Ω	Maximum wave growth rate

Subscripts

a	air
f	fuel
g	gas
KH	Kelvin-Helmholtz model
l	liquid
RT	Rayliegh-Taylor model